Electric-Field-Driven Resistive Switching in the Dissipative Hubbard Model

Jiajun Li,[1] Camille Aron,[2,3] Gabriel Kotliar,[2] and Jong E. Han[1,*]
[1]Department of Physics, State University of New York at Buffalo, Buffalo, New York 14260, USA
[2]Department of Physics, Rutgers University, Piscataway, New Jersey 08854, USA
[3]Department of Electrical Engineering, Princeton University, New Jersey 08455, USA
(Received 1 October 2014; revised manuscript received 16 January 2015; published 4 June 2015)

We study how strongly correlated electrons on a dissipative lattice evolve out of equilibrium under a constant electric field, focusing on the extent of the linear regime and hysteretic nonlinear effects at higher fields. We access the nonequilibrium steady states, nonperturbatively in both the field and the electronic interactions, by means of a nonequilibrium dynamical mean-field theory in the Coulomb gauge. The linear response regime, limited by Joule heating, breaks down at fields much smaller than the quasiparticle energy scale. For large electronic interactions, strong but experimentally accessible electric fields can induce a resistive switching by driving the strongly correlated metal into a Mott insulator. We predict a nonmonotonic upper switching field due to an interplay of particle renormalization and the field-driven temperature. Hysteretic I-V curves suggest that the nonequilibrium current is carried through a spatially inhomogeneous metal-insulator mixed state.

DOI: 10.1103/PhysRevLett.114.226403 PACS numbers: 71.27.+a, 71.30.+h, 72.20.Ht

The understanding of solids driven out of equilibrium by external fields [1,2] has been one of the central goals in condensed matter physics for the past century and is very relevant to nanotechnology applications such as resistive transitions. Multiple studies of this phenomenon have been performed in semiconductors and oxides [3–10]. In oxides, the application of an electric field can lead to a dramatic drop of resistivity up to 5 orders of magnitude. The relatively accessible threshold fields $E_{\rm th} \sim 10^{4-6}$ V/m and the hysteretic I-V curves make them good candidates for the fabrication of novel electronic memories. A Landau-Zener type of mechanism [11] seems unlikely as it predicts a threshold field on the order of 10^{8-9} V/m. In narrow gap chalcogenide Mott insulators, an avalanche breakdown was suggested with $E_{\rm th} \sim E_{\rm gap}^{2.5}$ [3]. Yet, the resistive switchings in other classes of correlated materials do not seem to involve solely electronic mechanisms. In organic charge-transfer complexes, it is believed to occur via the electrochemical migration of ions [4,5]. Finally, there are strong indications that a Joule heating mechanism occurs in some binary oxides such as NiO [7] and VO_2 [8–10]: the electric-field-driven current locally heats up the sample which experiences a temperature-driven resistive switching.

These experiments raise basic questions of how a strongly correlated state continuously evolves out of equilibrium under an external field, and how we describe the nonequilibrium steady states that consequently emerge. We develop a much needed basic microscopic theory of the driven metal-insulator transition.

Building on earlier theoretical efforts [11–27], we identify, in a canonical model of strongly interacting electrons, a region where electric-field-driven resistive switching takes place. We demonstrate how Joule heating effects modify the linear response regime and how, away from the linear regime, the same Joule physics leads to the hysteretic resistive transitions of the strongly correlated system. The derived energy scales for resistive transitions are orders of magnitude smaller than bare model parameters and belong within the feasible experimental range.

We study the Hubbard model in a constant and homogeneous electric field $\mathbf{E}$ which induces electric current $\mathbf{J}$. After a transient regime, a nonequilibrium steady state establishes if the power injected in the system, $\mathbf{J}\cdot\mathbf{E}$, is balanced by coupling the system to a thermostat which can absorb the excess of energy via heat transfer [14,15,21–24]. The thermostat is modeled by identical fermion reservoirs attached to each tight-binding (TB) site. In the Coulomb gauge, the electric field amounts in an electrostatic potential $-\ell E$ imposed on the ℓth TB site ($\ell = -\infty, \ldots, \infty$) and on its associated fermion bath [15]. The model is fully consistent with gauge-covariant models [23]. The noninteracting Hamiltonian reads

$$\begin{aligned}\hat{H}_0 = &-\gamma\sum_{\ell\sigma}(d^\dagger_{\ell+1,\sigma}d_{\ell\sigma} + \text{H.c.}) \\ &- \frac{g}{\sqrt{V}}\sum_{\ell\alpha\sigma}(d^\dagger_{\ell\sigma}c_{\ell\alpha\sigma} + \text{H.c.}) + \sum_{\ell\alpha\sigma}\epsilon_\alpha c^\dagger_{\ell\alpha\sigma}c_{\ell\alpha\sigma} \\ &- \sum_{\ell\sigma}\ell E\left(d^\dagger_{\ell\sigma}d_{\ell\sigma} + \sum_\alpha c^\dagger_{\ell\alpha\sigma}c_{\ell\alpha\sigma}\right), \end{aligned} \tag{1}$$

where $d^\dagger_{\ell\sigma}$ are the tight-binding electron creation operators at the ℓth site with spin $\sigma = \uparrow$ or $\downarrow$, and $c^\dagger_{\ell\alpha\sigma}$ are the corresponding reservoir electron operators attached. α is a continuum index corresponding to the reservoir dispersion relation ϵ_α defined with respect to the electrostatic potential

$-\ell E$. g is the overlap between the TB chain and the reservoirs of length V which will be sent to infinity. We assume that the reservoirs remain in equilibrium at bath temperature T_b. Later, we will extend this chain into a higher dimensional lattice. The electric field does not act within each reservoir whose role is to extract energy but not electric charge from the system [15]. We use a flat density of states (infinite bandwidth) for the reservoir spectra, and define the damping parameter as $\Gamma = V^{-1}\pi g^2 \sum_\alpha \delta(\epsilon_\alpha)$. We work with $\hbar = e = k_B = a = 1$ in which e is the electronic charge and a is the lattice constant. In the rest of this Letter, we measure energies in units of the full TB bandwidth $W = 4\gamma = 1$ (1D) and $W = 12\gamma = 1$ (3D). The exact solution of the noninteracting model in Eq. (1) has been shown [14,15] to reproduce the conventional Boltzmann transport theory despite the lack of momentum transfer scattering. The Hubbard model $\hat{H} = \hat{H}_0 + \hat{H}_1$ is defined with the on-site Coulomb interaction parameter U as

$$\hat{H}_1 = U \sum_\ell \left(d^\dagger_{\ell\uparrow} d_{\ell\uparrow} - \frac{1}{2} \right) \left(d^\dagger_{\ell\downarrow} d_{\ell\downarrow} - \frac{1}{2} \right). \tag{2}$$

Our calculations are in the particle-hole symmetric limit.

We use the dynamical mean-field theory (DMFT [16,28]) to treat the many-body interaction via a self-consistent local approximation of the self-energies. Note that the self-energy has contributions from both the many-body interaction $\hat{H}_1$ and the coupling to the reservoirs: $\Sigma^r_{\rm tot}(\omega) = -i\Gamma + \Sigma^r_U(\omega)$ and $\Sigma^<_{\rm tot}(\omega) = 2i\Gamma f_{\rm FD}(\omega) + \Sigma^<_U(\omega)$ with the Fermi-Dirac (FD) distribution $f_{\rm FD}(\omega) \equiv [1 + \exp(\omega/T_b)]^{-1}$. Once the local retarded and lesser self-energies are computed, one can access the full retarded and lesser Green's functions (GFs). Note that, in a homogeneous nonequilibrium steady state, all the TB sites are equivalent. In the Coulomb gauge, this leads to $G^{r,<}_{\ell\ell'}(\omega) = G^{r,<}_{\ell+k,\ell'+k}(\omega + kE)$ and similarly for the self-energies [15,25], as can be derived via a gauge transformation from the temporal gauge.

Below, we present the implementation of our DMFT scheme in the Coulomb gauge directly in the steady states. It consists in singling out one TB site—say $\ell = 0$—(often referred as impurity) and replacing its direct environment (i.e., semi-infinite dissipative Hubbard chains and its own reservoir) with a self-consistently determined noninteracting environment (often referred as Weiss "fields"). The local electronic problem is then treated by means of an impurity solver.

For a given self-energy $[\Sigma^{r,<}_\ell(\omega) \equiv \Sigma^{r,<}_U(\omega + \ell E)]$, the on-site Green's functions obey the following Dyson equations:

$$G^r(\omega)^{-1} = \omega - \Sigma^r_{\rm tot}(\omega) - \gamma^2 F^r_{\rm tot}(\omega), \tag{3}$$

$$G^<(\omega) = |G^r(\omega)|^2 [\Sigma^<_{\rm tot}(\omega) + \gamma^2 F^<_{\rm tot}(\omega)], \tag{4}$$

in which $\gamma^2 F^{r,<}_{\rm tot}$ are the total hybridization functions to the left and right semi-infinite chains, $F^{r,<}_{\rm tot}(\omega) = F^{r,<}_+(\omega + E) + F^{r,<}_-(\omega - E)$. $F_+(\omega)$ is the on-site retarded GF at the end of the rhs chain ($\ell = 1$) which obeys the self-similar Dyson equation

$$F^r_+(\omega)^{-1} = \omega - \Sigma^r_{\rm tot}(\omega) - \gamma^2 F^r_+(\omega + E), \tag{5}$$

which can be solved recursively after more than 500 iterations. $F_-(\omega)$ corresponds to the GF of the lhs chain and can be obtained similarly. The noninteracting parts of the impurity GFs, $\mathcal{G}$, are constructed using

$$\mathcal{G}^r(\omega)^{-1} = \omega + i\Gamma - \gamma^2 F^r_{\rm tot}(\omega), \tag{6}$$

$$\mathcal{G}^<(\omega) = |\mathcal{G}^r(\omega)|^2 [2i\Gamma f_{\rm FD}(\omega) + \gamma^2 F^<_{\rm tot}(\omega)]. \tag{7}$$

The local self-energies are obtained by means of the iterative-perturbation theory up to the second-order in the Coulomb parameter U: $\Sigma^{\gtrless}_U(t) = U^2 [\mathcal{G}^{\gtrless}(t)]^2 \mathcal{G}^{\lessgtr}(t)$. The GFs are updated with this self-energy using the above Dyson's equations, and the procedure is repeated until convergence is achieved.

We generalize the above method to higher dimensions. With the electric field along the principal axis direction, $\mathbf{E} = E\hat{\mathbf{x}}$, the lattice is translation invariant in the perpendicular direction and the above construction of the Dyson's equation can be carried out independently per each perpendicular momentum vector. See Supplemental Material [29] for a detailed discussion. Below, we present results of the model in one and three dimensions.

First, we discuss the linear response regime. Within the DMFT, the dc conductivity in the limit of zero temperature and zero electric field can be obtained via the Kubo formula as $\sigma_{\rm dc} \propto \lim_{\omega\to 0} \sum_{\mathbf{k}} \int d\nu \rho_{\mathbf{k}}(\nu) \rho_{\mathbf{k}}(\nu + \omega) [f_{\rm FD}(\nu) - f_{\rm FD}(\nu + \omega)]/\omega = \sum_{\mathbf{k}} \int d\nu [\rho_{\mathbf{k}}(\nu)]^2 \delta(\nu)$ with the spectral function at a given wave vector $\mathbf{k}$, $\rho_{\mathbf{k}}(\nu) = -\pi^{-1} {\rm Im}[\nu - \epsilon_{\mathbf{k}} + i\Gamma - \Sigma^r_U(\nu)]^{-1}$. Therefore, as long as $\Sigma^r_U(\nu) \to 0$ as $\nu \to 0, T \to 0$, the dc conductivity is independent of the interaction. This argument is similar to the one used by Prange and Kadanoff [30] for the electron-phonon interaction. Recent calculations did not have access to the linear response regime [21,23,24].

Figure 1 confirms the validity of the linear response analysis. The initial slope of the J-E relation is independent of the interaction strength U [26] both in (a) one and (b) three dimensions. The linear behavior deviates at the field $E_{\rm lin} \approx 0.003$ in (a), orders of magnitude smaller than the renormalized bandwidth $W^* = zW \approx 0.5$ with the equilibrium renormalization factor $z = [1 - {\rm Re}\partial\Sigma^r_U(\omega)/\partial\omega]^{-1}_{\omega = E = T_b = 0}$.

With an increasing E field, the contribution at $E = U/2$ is a two-step resonant process which can be viewed as a consequence of the energy overlap between the lower or upper Hubbard bands of the left or right neighboring sites

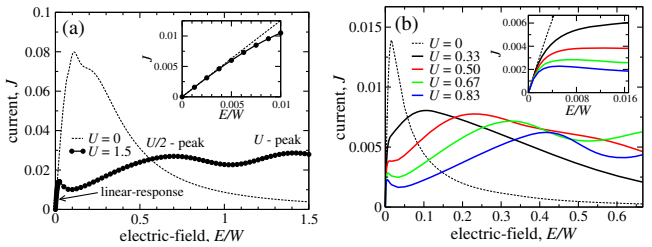

FIG. 1 (color online). Electric current (per spin) J vs electric field E. (a) 1D chain with damping $\Gamma = 0.0625W$ and fermion bath temperature $T_b = 0.001\,25W$ with the 1D TB bandwidth $W = 4\gamma$. The linear conductance in the small field limit (magnified in the inset) is the same for noninteracting ($U = 0$) and interacting ($U = 1.5W$) models. After the conductivity deviates from the linear response behavior, inelastic contributions appear at $E = U/2$ and $E = U$. (b) 3D lattice with $\Gamma = 0.0083W$ and $T_b = 0.000\,42W$ with the 3D TB bandwidth $W = 12\gamma$. The main features remain similar to the 1D case. All following energies are in units of W, unless otherwise mentioned.

with the in-gap states present at the Fermi level [27]. The current peak at $E = U$ is due to the direct overlap of the Hubbard bands on neighboring sites [18,27].

The immediate departure from the linear conductivity at very small fields can be well understood with a Joule heating scenario in which the Coulombic interaction is the dominant scattering process and is rapidly modified by an increasing effective temperature as the field is increased. First, we demonstrate this effective temperature effect by showing, in Fig. 2(a), that the scattering rates from the Coulomb interaction, $\tau_U^{-1} = -\mathrm{Im}\Sigma_U^r(\omega = 0)$, for different sets of the damping Γ, collapse onto a scaling curve as a function of $(E/\Gamma)^2$ for small E. This scaling is clearly evocative of the well-known T^2 behavior of equilibrium retarded self-energies.

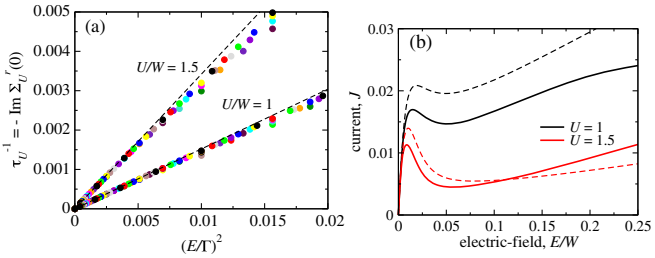

FIG. 2 (color online). (a) Interacting scattering rate, $\tau_U^{-1} = -\mathrm{Im}\Sigma_U^r(\omega = 0)$, plotted against $(E/\Gamma)^2$. Different colors denote different damping $\Gamma = 0.0125, \ldots, 0.06$ with the interval of 0.0025. For small (E/Γ), the numerical results on the 1D chain collapse on well-defined lines at $U = 1$ and 1.5. The dashed lines are predictions based on the equilibrium self-energy with the temperature replaced by the noninteracting effective temperature T_{eff} given in Eq. (8). The remarkable agreement proves that Joule heating controls the scattering in the small field limit. (b) Comparison of the current and the Drude formula estimate with the total scattering rate $\Gamma + \tau_U^{-1}$, with qualitative agreement beyond the linear response limit.

In the noninteracting 1D chain with $T_b = 0$, the effective temperature has been obtained in the small field limit as [15,17]

$$T_{\mathrm{eff}} = \frac{\sqrt{6}}{\pi}\gamma\frac{E}{\Gamma}. \tag{8}$$

Inserting this T_{eff} into the equilibrium perturbative self-energy [31], we obtain, in the weak-U limit,

$$\tau_U^{-1} = -\mathrm{Im}\Sigma_{\mathrm{eq}}^r(\omega = 0, T_{\mathrm{eff}}) \approx \frac{\pi^3}{2}A_0(0)^3U^2T_{\mathrm{eff}}^2, \tag{9}$$

which is represented by the dashed lines in Fig. 2(a). Here, $A_0(0) = (\pi\sqrt{\Gamma^2 + 4\gamma^2})^{-1}$ is the noninteracting DOS at $\omega = 0$. The robust agreement in the self-energies leaves no doubt that the electron scattering is dominated by the Joule heating with T_{eff} given with Eq. (8) in the linear response limit in the presence of interaction. T_{eff} then deviates strongly from this behavior outside the narrow linear regime, as discussed below.

The scattering rate can be directly related to the electric current via the Drude conductivity $J(E) = \sigma_{\mathrm{dc}}(E)E$ with the nonlinear dc conductivity $\sigma_{\mathrm{dc}}(E)$. In the noninteracting limit, the linear conductivity can be written as $\sigma_{0,\mathrm{dc}} = 2\gamma^2/(\pi\Gamma\sqrt{\Gamma^2 + 4\gamma^2})$ [15]. In Fig. 2(b), we plot the Drude formula with the scattering rate Γ replaced by the total scattering $\Gamma_{\mathrm{tot}} = \Gamma + \tau_U^{-1}$. The qualitative agreement with the numerical results extends over a wide range of the E field, well beyond the linear regime.

Using Eq. (9), the current at the small field can be approximated as $J = \sigma_{0,\mathrm{dc}}E/(1 + E^2/E_{\mathrm{lin}}^2)$ with the departure from the linear behavior occurring around (from the condition $\Gamma \approx \tau_U^{-1}$ at $E = E_{\mathrm{lin}}$), $E_{\mathrm{lin}} \approx (8\pi^2/3)^{1/2}\gamma^{1/2}\Gamma^{3/2}/U$. This estimate is valid away from $U = 0$ and the metal-insulator limit, and agrees well with Fig. 2(b) [32]. We emphasize that, while negative-differential-resistance (NDR) behaviors typically occur in periodic structures due to the Bloch oscillations [33] as shown by the dashed lines ($U = 0$) in Fig. 1, the NDR here comes from strong nonlinear scattering enhanced by the Joule heating.

In the presence of weak dissipation and strong electronic interactions, the nonequilibrium evolution becomes more dramatic. With the effective temperature, Eq. (8), having a singular limit as $\Gamma \to 0$, the electron temperature tends to rise very sharply as the field is applied. This effect, together with a small value of the renormalized coherent energy scales, causes the system to immediately deviate from the linear response regime, preventing itself from overheating. This mechanism, in a vicinity of a quantum phase transition, can strongly modify the state of a system. Indeed, we will show that there is a region of the parameters U and E for which the nonequilibrium Dyson's equations have two distinct solutions, one corresponding to an incoherent metal and the other to an insulator.

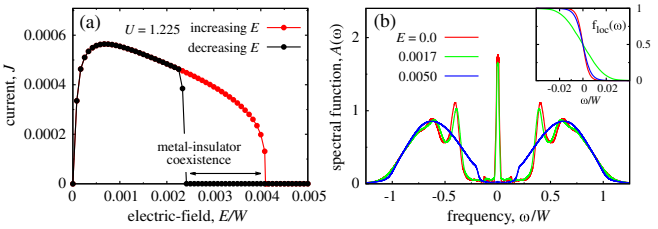

FIG. 3 (color online). (a) Electric-field-driven metal-to-insulator transition (MIT) in the vicinity of a Mott-insulator at $U = 1.225$, $\Gamma = 0.00167$ and $T_b = 0.0025$ in a 3D cubic lattice with the electric field in the x direction. The metallic state at zero field becomes insulating at an electric field of magnitude orders of magnitude smaller than bare energy scales. Depending on whether the electric field is increased or decreased, metal-insulator hysteresis occurs with a window for phase-coexistence. (b) Spectral function and distribution function $f_{\rm loc}(\omega)$ with an increasing electric field. The quasiparticle (QP) spectral weight rapidly disappears near the MIT driven by the electric field, opening an insulating gap. The nonequilibrium energy distribution function indicates that the system undergoes a highly nonmonotonic cold-hot-cold temperature evolution near the MIT.

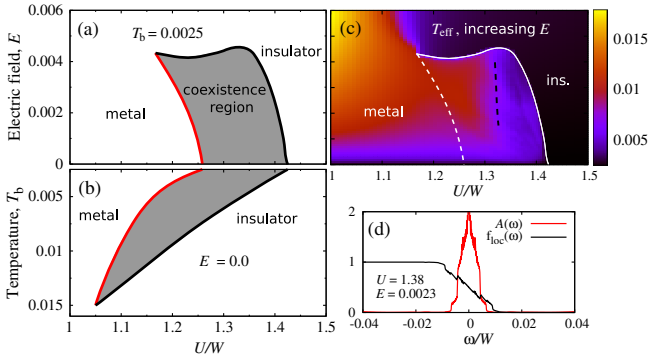

FIG. 4 (color online). Phase diagram of the metal-insulator transition in a cubic lattice driven by (a) electric field and (b) temperature. The metal-insulator coexistent phase exists between the metal-to-insulator transition (black line) with increasing E or T_b, and the insulator-to-metal transition (red line) with decreasing E or T_b. $\Gamma = 0.001\,67$. (c) Effective temperature $T_{\rm eff}$ map with increasing E, with the white line for the MIT. The white dashed line becomes the phase boundary with a decreasing field. (d) Spectral and distribution functions for strong U beyond the crossover line [black dashed line in (c)]. Quasiparticle states are disconnected from incoherent spectra and their statistical property becomes strongly nonthermal.

In Fig. 3(a), we start from a metallic state at $U = 1.225$, and increase the electric field from zero. We use the self-consistent solution at a certain E field as an input to the next E run. As discussed above, the system has an extremely narrow linear response window with $E_{\rm lin} \sim 10^{-4}$, followed by an NDR behavior. As the electric field is further increased, an electric-field-driven metal-to-insulator RS occurs at $E_{\rm MIT} \approx 0.004$. Similar strong nonlinear I-V behavior followed by a resistive transition has been observed in NiO [7]. After gradual changes in the spectral functions in Fig. 3(b), a finite insulating gap opens abruptly after the RS. The local energy distribution function $f_{\rm loc}(\omega)$, defined as $f_{\rm loc}(\omega) = -\frac{1}{2}{\rm Im}G^<(\omega)/{\rm Im}G^r(\omega)$, evolves from the FD function at zero field to a shape with a high effective temperature. At the RS, the Joule heating nearly stops and the TB lattice goes back to the low temperature state [34]. We emphasize that the energy scale hierarchy

$$E_{\rm lin} \ll E_{\rm MIT} \ll W^* \tag{10}$$

differs markedly from that in the quantum dot transport [35] in which the dissipation occurs outside the quantum dot region and the bias scale for decoherence is comparable to the QP energy scale.

Figures 4(a) and 4(b) show the metal-insulator coexistence. Our estimate of the threshold electric field $E_{\rm MIT} \approx 0.004$ at $U = 1.225$ can be converted to $E_{\rm MIT} = 10^7 - 10^8$ V/m if $U = 1$–10 eV. Based on the balance between the Joule heating and the dissipation [15,36], a scaling argument [29] implies that the critical field decreases with damping as $E_{\rm MIT} \propto \sqrt{\Gamma}$. Therefore, accounting for the range of experimental threshold fields would require Γ on the order of 10^{-3} meV. We stress that the model successfully captures, at a microscopic level, the qualitative features of the resistive switching phenomenon, but a more quantitative analysis calls for a better modeling of the dissipative mechanisms.

While the phase diagram for the RS of Fig. 4(a) generally reflects that of the equilibrium MIT [28] in (b), the upturn of the upper critical E field (black line) in Fig. 4(a) with increasing U is counterintuitive. This originates from an interplay of different scaling regimes for large and small U separated by the crossover line (dashed line) at about $U_{\rm cross}/W \approx 1.32$. For small $U < U_{\rm cross}$, the QP bandwidth W^* is larger than $T_{\rm eff}$, and the scaling relation $T_{\rm eff} \propto \sqrt{E/U}$ [29] is obtained far from the linear regime, Eq. (8). However, for $U > U_{\rm cross}$ with $W^* \lesssim T_{\rm eff}$, $T_{\rm eff}$ increases with E very weakly [29], as seen in Fig. 4(c). This slow increase of $T_{\rm eff}$ allows a larger critical field and leads to the maximum $E_{\rm MIT}(U)$ near $U = U_{\rm cross}$—a prediction which can be experimentally verified. The spectral and distribution functions in Fig. 4(d) for $U > U_{\rm cross}$, show the QP states with spectrally disconnected incoherent electrons, and a strong nonthermal behavior even at $E/W^* \sim 0.1$. To evaluate $T_{\rm eff}$, a fit to a Fermi-Dirac function with $T_{\rm eff}$ has been performed on data satisfying $|f_{\rm loc}(\omega) - 0.5| < 0.25$.

Even though the calculations performed here are on homogeneous lattices, the phase coexistence suggests that, under a uniform field, the system can be spatially segregated into metal and insulator regions which, in turn, have inhomogeneous temperature distribution with complex thermodynamic states. The hot metallic regions will be oriented in the direction of the field, forming experimentally observed current-carrying filaments.

The Joule heating scenario has been previously invoked in the literature for resistive switching in disordered films [36]. Our calculations of the coexistence of two distinct nonequilibrium steady-state solutions in the framework of a relatively simple quantum mechanical model could be applicable to NiO [7] and $Cr_xV_{2-x}O_3$ [37] systems where metal-to-insulator transitions occur with increasing temperature. Our calculation ignores long-range antiferromagnetic correlations and does not address switching from ordered insulating phases. Further extensions to cluster-DMFT would allow a realistic treatment of the electronic structure and could successfully address the case of VO_2.

The authors are grateful for helpful discussions with Satoshi Okamoto, Sambandamurthy Ganapathy, and Sujay Singh. This work has been supported by the National Science Foundation through Grants No. DMR-0907150, No. DMR-115181, No. DMR-1308141, No. PHYS-1066293, and by the hospitality of the Aspen Center for Physics.

*jonghan@buffalo.edu

[1] L. P. Kadanoff and G. Baym, *Quantum Statistical Mechanics* (Westview Press, New York, 1994).
[2] G. D. Mahan, *Many-Particle Physics*, Physics of Solids and Liquids, 3rd ed. (Kluwer Academic, New York, 2000), Chap. 8.
[3] V. Guiot, L. Cario, E. Janod, B. Corraze, V. Ta Phuoc, M. Rozenberg, P. Stoliar, T. Cren, and D. Roditchev, Nat. Commun. **4**, 1722 (2013); P. Stoliar, L. Cario, E. Janod, B. Corraze, C. Guillot-Deudon, S. Salmon-Bourmand, V. Guiot, J. Tranchant, and M. Rozenberg, Adv. Mater. **25**, 3222 (2013).
[4] R. Kumai, Y. Okimoto, and Y. Tokura, Science **284**, 1645 (1999).
[5] J. Jeong, N. Aetukuri, T. Graf, T. D. Schladt, M. G. Samant, and S. S. P. Parkin, Science **339**, 1402 (2013).
[6] S. Lee, A. Fursina, J. T. Mayo, C. T. Yavuz, V. L. Colvin, R. G. Sumesh Sofin, I. V. Shvets, and D. Natelson, Nat. Mater. **7**, 130 (2007).
[7] S. B. Lee, S. C. Chae, S. H. Chang, J. S. Lee, S. Park, Y. Jo, S. Seo, B. Kahng, and T. W. Noh, Appl. Phys. Lett. **93**, 252102 (2008).
[8] J. Duchene, M. Terraillon, P. Pailly, and G. Adam, Appl. Phys. Lett. **19**, 115 (1971).
[9] T. Driscoll, H.-T. Kim, B.-G. Chae, M. Di Ventra, and D. N. Basov, Appl. Phys. Lett. **95**, 043503 (2009).
[10] A. Zimmers, L. Aigouy, M. Mortier, A. Sharoni, Siming Wang, K. G. West, J. G. Ramirez, and I. K. Schuller, Phys. Rev. Lett. **110**, 056601 (2013).
[11] T. Oka, R. Arita, and H. Aoki, Phys. Rev. Lett. **91**, 066406 (2003); T. Oka and H. Aoki, Phys. Rev. B **81**, 033103 (2010); T. Oka, Phys. Rev. B **86**, 075148 (2012).
[12] V. Turkowski and J. K. Freericks, Phys. Rev. B **71**, 085104 (2005).
[13] J. K. Freericks, Phys. Rev. B **77**, 075109 (2008).
[14] J. E. Han, Phys. Rev. B **87**, 085119 (2013).
[15] J. E. Han and J. Li, Phys. Rev. B **88**, 075113 (2013).
[16] H. Aoki, N. Tsuji, M. Eckstein, M. Kollar, T. Oka, and P. Werner, Rev. Mod. Phys. **86**, 779 (2014).
[17] A. Mitra and A. J. Millis, Phys. Rev. B **77**, 220404(R) (2008).
[18] A. V. Joura, J. K. Freericks, and Th. Pruschke, Phys. Rev. Lett. **101**, 196401 (2008).
[19] M. Eckstein, T. Oka, and P. Werner, Phys. Rev. Lett. **105**, 146404 (2010).
[20] N. Sugimoto, S. Onoda, and N. Nagaosa, Phys. Rev. B **78**, 155104 (2008).
[21] N. Tsuji, T. Oka, and H. Aoki, Phys. Rev. B **78**, 235124 (2008).
[22] M. Mierzejewski, L. Vidmar, J. Bonca, and P. Prelovsek, Phys. Rev. Lett. **106**, 196401 (2011); L. Vidmar, J. Bonca, T. Tohyama, and S. Maekawa, *ibid.* **107**, 246404 (2011).
[23] C. Aron, G. Kotliar, and C. Weber, Phys. Rev. Lett. **108**, 086401 (2012).
[24] A. Amaricci, C. Weber, M. Capone, and G. Kotliar, Phys. Rev. B **86**, 085110 (2012).
[25] Satoshi Okamoto, Phys. Rev. Lett. **101**, 116807 (2008).
[26] G. Mazza, A. Amaricci, M. Capone, and M. Fabrizio, Phys. Rev. B **91**, 195124 (2015).
[27] C. Aron, Phys. Rev. B **86**, 085127 (2012).
[28] A. Georges, G. Kotliar, W. Krauth, and M. J. Rozenberg, Rev. Mod. Phys. **68**, 13 (1996).
[29] See Supplemental Material at http://link.aps.org/supplemental/10.1103/PhysRevLett.114.226403 for detailed derivation of the Dyson equations and discussions of scaling behaviors in resistive switching.
[30] R. E. Prange and L. P. Kadanoff, Phys. Rev. **134**, A566 (1964).
[31] K. Yamada, Prog. Theor. Phys. **54**, 316 (1975).
[32] In a more realistic model with impurity scattering which becomes more effective than the dissipation at small fields, the critical field has different behavior $E_{\rm lin} \propto \tau_{\rm imp}^{-1/2}\Gamma/U$.
[33] Paul A. Lebwohl and Raphael Tsu, J. Appl. Phys. **41**, 2664 (1970).
[34] At the metal-to-insulator RS, the $T_{\rm eff}$ cools as far as the insulating state is allowed as a metastable solution in the equilibrium phase diagram, Fig. 4(b). Therefore, the $T_{\rm eff}$ at the E field immediately after the upper switching field $E_{\rm MIT}$ maps to the red line in Fig. 4(b). After the RS to insulator, the current, while reduced by orders of magnitude, self-consistently produces the Joule heat enough to support the insulating solution. See also Fig. 4(c).
[35] D. Goldhaber-Gordon, Hadas Shtrikman, D. Mahalu, David Abusch-Magder, U. Meirav, and M. A. Kastner, Nature (London) **391**, 156 (1998); S. M. Cronenwett, T. H. Oosterkamp, and L. P. Kouwenhoven, Science **281**, 540 (1998).
[36] B. L. Altshuler, V. E. Kravtsov, I. V. Lerner, and I. L. Aleiner, Phys. Rev. Lett. **102**, 176803 (2009).
[37] D. B. McWhan, A. Menth, J. P. Remeika, W. F. Brinkman, and T. M. Rice, Phys. Rev. B **7**, 1920 (1973); P. Hansmann, A. Toschi, G. Sangiovanni, T. Saha-Dasgupta, S. Lupi, M. Marsi, and K. Held, Phys. Status Solidi B **250**, 1251 (2013).